Rios X, Compte M, Gómez-Vallejo V, et al. Immuno-PET imaging and pharmacokinetics of an anti-CEA scFv-based trimerbody and its monomeric counterpart in human gastric carcinoma-bearing mice. Molecular Pharmaceutics. 2019. doi: 10.1021/acs.molpharmaceut.8b01006

Immuno-PET imaging and pharmacokinetics of an anti-CEA scFv-based trimerbody and its monomeric counterpart in human gastric carcinoma-bearing mice

Xabier Rios,[a, †] Marta Compte,[b, †] Vanessa Gómez-Vallejo,[c] Unai Cossío,[a] Zuriñe Baz,[a] Miguel Ángel Morcillo,[d] Pedro Ramos-Cabrer,[e,f] Luis Alvarez-Vallina,[g] Jordi Llop,[a,]*

[a]Radiochemistry and Nuclear Imaging Group, CIC biomaGUNE, 20014 San Sebastián, Guipúzcoa, Spain.

[b]Molecular Immunology Unit, Hospital Universitario Puerta de Hierro Majadahonda, Manuel de Falla 1, 28222 Majadahonda, Madrid, Spain

[c]Radiochemistry Platform, CIC biomaGUNE, 20014 San Sebastián, Guipúzcoa, Spain.

[d]Biomedical Applications of Radioisotopes and Pharmacokinetics Unit, CIEMAT, 28040 Madrid, Spain

[e] Magnetic Resonance Imaging Group, CIC biomaGUNE, 20014 San Sebastián, Guipúzcoa, Spain

[f]Ikerbasque, The Basque Foundation for Science, Bilbao, Spain

[g]Immunotherapy and Cell Engineering Group, Department of Engineering, Aarhus University, Gustav WiedsVej 10, 8000 C Aarhus, Denmark

[†] These authors contributed equally to this work

ABSTRACT GRAPHIC

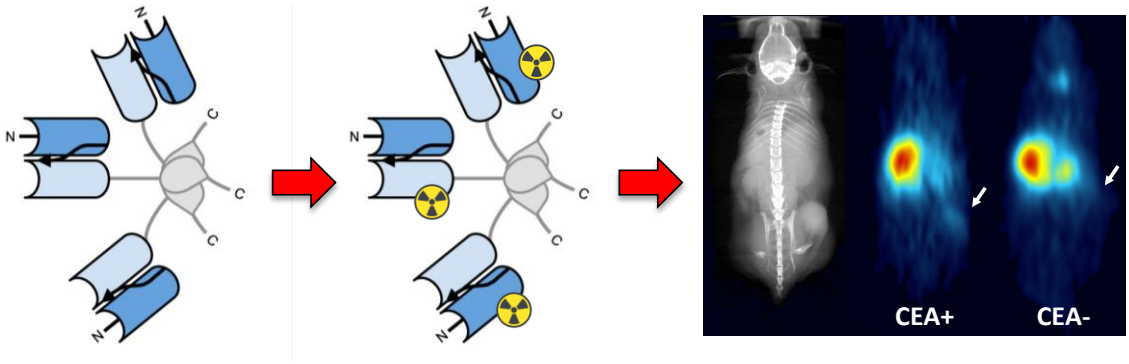

ABSTRACT

Monoclonal antibodies (mAbs) are currently used as therapeutic agents in different types of cancer. However, mAbs and antibody fragments developed so far show suboptimal properties in terms of circulation time and tumor penetration/retention. Here, we report the radiolabeling, pharmacokinetic evaluation, and determination of tumor targeting capacity of the previously validated anti-CEA MFE23-scFv-based N-terminal trimerbody (MFE23^{N}-trimerbody), and the results are compared to those obtained for the monomeric MFE23-scFv. Dissection and gamma-counting studies performed with the ^{131}I-labeled protein scaffolds in normal mice showed slower blood clearance for the trimerbody, and accumulation in the kidneys, the spleen and the liver for both species. These, together with a progressive uptake in the small intestine, confirm a combined elimination scheme with hepatobiliary and urinary excretion. Positron emission tomography studies performed in a xenograft mouse model of human gastric adenocarcinoma, generated by subcutaneous administration of CEA-positive human MKN45 cells, showed higher tumor accumulation and tumor-to-muscle (T/M) ratios for ^{124}I-labeled MFE23^{N}-trimerbody than for MFE23-scFv. Specific uptake was not detected with PET imaging in CEA negative xenografts as indicated by low T/M ratios. Our data suggest that engineered intermediate-sized trivalent antibody fragments could be promising candidates for targeted therapy and imaging of CEA-positive tumors.

KEYWORDS

Carcinoembryonic antigen; Single-chain variable fragment; Trimerbody; Positron Emission Tomography; PET; Radiolabeling

INTRODUCTION

Cancer is a leading cause of death, with 14 million new cases and 8.2 million cancer-related deaths worldwide in 2012.[1] Hence, the development of new tools for the early diagnosis and treatment of cancer is urgently required. Among the different therapeutic strategies, the use of monoclonal antibodies (mAbs) and their mAb-derived fragments have received considerable attention in the last decades.[2]

Antibody fragments designed for *in vivo* tumor targeting should have high specificity and affinity for the target antigen and low immunogenicity, together with rapid clearance from blood and low accumulation in healthy tissues.[3] Indeed, the pharmacokinetic properties are mainly driven by format and molecular weight. For example, intact IgG molecules with a size of approximately 150 kDa diffuse slowly, and display long half-life in blood and incomplete tumor penetration which is restricted to perivascular tumor regions.[4] Single-chain variable fragments (scFvs; 25-30 kDa) are single gene products that include both the heavy chain and light chain variable domains (V_H and V_L) of an antibody separated by a flexible linker. Such fragments retain the specificity of the parental antibodies but have faster clearance and decreased affinity because of their monovalency.[5] Another class of antibody fragment is the nanobody, or single-domain antibody (sdAb), typically derived from camelid heavy chain-only antibodies (V_{HH}) or camelized human V_H libraries, with a size of 12-15 kDa.[6] Like scFvs, sdAbs have better tumor penetration properties than intact antibodies but renal clearance occurs fast and tumor retention is low due to their monovalent binding properties.[7]

It is well established that bivalent antibodies, i.e. diabodies (55 kDa) might be better candidates to image tumors, as they show higher total tumor uptake and improved tumor-to-blood ratios than intact IgG molecules,[8] thanks to their bivalency and higher avidity.[9] Likewise,

minibodies (80 kDa) which result from the fusion of scFv with the human IgG1 C_{H3} domain, show longer half-life but relatively rapid uptake in tumors.[10]

In the pursuit of antibody-based molecules with improved tumor targeting and retention capacity, we have previously generated a new class of multivalent antibodies made by fusing a human collagen XVIII-derived trimerization domain (TIE) to the N- or C-terminus of a scFv fragment.[11-12] The new antibody format, termed trimerbody, is an intermediate-sized (110 kDa) trivalent molecule with good stability under physiological conditions[13] and enhanced binding capacity through multivalency, providing thus a significant increase in functional affinity and slower dissociation.[13-14] As previously demonstrated, the near-infrared fluorescently labeled carcinoembryonic antigen (CEA)-specific MFE23 scFv-based N-terminal trimerbody ($MFE23^{N}$-trimerbody) can specifically localize CEA-expressing xenografts.[14]

Moving forward towards a potential translation into the clinical setting, in the current work we evaluate the tumor targeting capacity of the anti-CEA $MFE23^{N}$-trimerbody using positron emission tomography (PET) imaging. With that aim, the $MFE23^{N}$-trimerbody was labeled with Iodine-124 (^{124}I) and imaging sessions were conducted at different time points after intravenous administration into a xenograft mouse model of gastric adenocarcinoma, generated by subcutaneous administration of CEA-positive human MKN45 cells, which show medium-high CEA expression as previously shown in the literature.[15] As negative control, CEA-negative human fibrosarcoma HT1080 cells were used. Tumor uptake was compared to that obtained with the monovalent counterpart, ^{124}I-MFE23-scFv. Complementary experiments in non-tumor bearing mice using dissection and gamma counting were conducted with the ^{131}I-labeled antibody scaffolds, to obtain pharmacokinetic data and accurately determine whole body biodistribution and blood clearance.

MATERIALS AND METHODS

Cells and culture conditions

Cells (HEK-293, human embryo kidney epithelia, CRL-1573, ATTC; HT-1080, human fibrosarcoma, CCL-121, ATTC; and MKN45, human stomach adenocarcinoma, JCRB-0254, Cellbank Australia) were routinely screened for the absence of mycoplasma contamination using the Mycoplasma Plus TM Primer Set (Stratagene, Cedar Creek, TX, USA). Cells were cultured in Dulbecco's modified Eagle's medium (DMEM) (Lonza, Walkersville, MD, USA) supplemented with 2 mM L-glutamine, 10% (vol/vol) heat-inactivated fetal calf serum (FCS), and antibiotics (100 units/mL penicillin, 100 mg/mL streptomycin) (all from Life Technologies, Carlsbad, CA, USA).

Construction of expression vectors

The mammalian expression vector pCEP4-MFE23-hNC1 encoding the CEA-specific MFE23 scFv-based *N*-terminal trimerbody has been previously described.[14] To generate the bacterial expression plasmid pAB1-MFE23-scFv a synthetic gene encoding the MFE23-scFvwas synthesized by Geneart AG (Regensburg, Germany), and the *Nco*I/*Not*I cleaved fragment was ligated into the pUC19-derived bacterial expression vector pAB1.[16]

Expression and purification of recombinant antibodies

MFE23-scFv was produced as described before.[17] For the production of the MFE23^{N}-trimerbody, HEK-293 cells were transfected with the pCEP4-MFE23-hNC1 expression vectors using calcium phosphate[18] and selected in complete medium with 200 μg/ml hygromycin B (Life Technologies) to generate stable cell lines. To purify the MFE23^{N}-trimerbody, serum-free conditioned medium was collected from stably transfected cell lines, centrifuged, filtered,

dialyzed against PBS (pH 7.4) and loaded onto a 1 ml HisTrap HP column using and ÄKTA Prime plus system. The resulting fractions from both purifications were pooled, dialyzed against PBS, and concentrated using spin trap columns (Merck Millipore, Billerica, MA, USA).

Flow cytometry

Cells were incubated with anti-CEA mAb (5 µg/ml) (clone C6G9; Sigma-Aldrich, San Louis, MO, USA) or MFE23 antibodies (MFE23-scFv or MFE23^{N}-trimerbody, at equimolar dose) and Tetra-His mAb (Qiagen, GmbH, Hilden, Germany) for 30 min on ice. After washing, the cells were treated with appropriate dilutions of phycoerytrin (PE)-conjugated goat F(ab')$_2$ anti-mouse IgG (Fc fragment specific, Jackson Immuno Research, Newmarket, UK). All samples were analyzed with a MacsQuant Analyzer 10 (Miltenyi Biotec, Bergisch Gladbach, Germany).

Radiochemistry

The radioiodination of the MFE23-scFv and the MFE23^{N}-trimerbody was carried out by electrophilic aromatic substitution on the tyrosine residues following a previously published method with modifications.[19] In brief, a solution of the MFE23-scFv or the MFE23^{N}-trimerbody (10 µg/10 µL) was incubated with Na[^{131}I]I (70 MBq, solution in 0.1M NaOH, Perkin Elmer) or Na[^{124}I]I (370 MBq, solution in 0.02M NaOH, Perkin Elmer, Waltham, MA, USA) in PBS (10 µL, 0.5 M, pH 7.4) for 20 min at 0°C into a iodination tube (Pierce™ Pre-Coated Iodination Tube, Thermo Scientific, Waltham, MA, USA). Gentle periodic shaking was applied. The crude was diluted with phosphate buffer solution (PBS, 250 µL, 0.01 M, containing NaCl 1 M, pH 7.4) and the resulting solution was transferred to a vial containing $Na_2S_2O_3$ (50µL, 0.1 M). Finally, PBS (250 µL, 0.1 M, containing 0.1% BSA and 1% NaI, pH 7.4) was added and the resulting solution was submitted to purification on a Sephadex™ Column (Illustra™ Nap™-5 Columns Sephadex™ G-25 DNA grade, GE Healthcare) using PBS (0.1 M, containing 0.1% BSA and 1%

NaI, pH 7.4) as the mobile phase.[20] The eluted product was collected in 100µL fractions, and those containing a higher concentration of radioactivity (see Fig. S1 for example of elution profile of the trimerbody) were subsequently used for *ex vivo/in vivo* experiments. Radiochemical yield was calculated as the ratio between the amount of radioactivity in the collected fractions and the starting amount of radioactivity. Specific activity was calculated as the ratio between the amount of activity in the collected fractions and the starting mass amount of MFE23-scFv or MFE23^{N}-trimerbody, and expressed in MBq/µmol. Radiochemical purity was determined by radio-thin layer chromatography (radio-TLC) using iTLC-SG chromatography paper (Agilent Technologies, CA, USA) and water/ethanol solution (15/85 v/v) as the stationary and mobile phases, respectively. TLC plates were analyzed using a TLC-reader (MiniGITA, Raytest). During set up of the experimental processes, radiochemical purity was also determined using radio-SDS-PAGE gel electrophoresis. The distribution of radioactivity in the gel was determined using the TLC-reader. Radiochemical stability of the labeled MFE23-scFv and MFE23^{N}-trimerbody were evaluated by incubating the labeled species in both physiologic saline solution and mouse plasma at 37°C. At different time points (1 and 24 h), samples were withdrawn and analyzed using TLC (samples incubated in saline solution) or radio-SDS-PAGE electrophoresis (samples incubated in plasma) under the experimental conditions described above.

Determination of immunoreactive fraction

The determination of the immunoreactive fraction of the labeled MFE23-scFv or MFE23^{N}-trimerbody was carried out following a modified Lindmo method[21] as previously reported.[22] In brief, cells were harvested by trypsinization, washed and resuspended in PBS at a concentrationof 5x10^{6} cells/mL. For each protein scaffold, five dilutions were performed in PBS

(pH = 7.4) to achieve concentrations in the range $5x10^5$- $5x10^6$ cells/mL and 0.5 mL of each concentration were introduced in plastic tubes. Two extra tubes containing $5x10^6$ cells/mL (0.5 mL) were also prepared to measure non-specific binding. Non-labeled MFE23-scFv or $MFE23^N$-trimerbody (100 µg) was added to the non-specific binding tubes and briefly vortex-mixed. Labeled MFE23-scFv or $MFE23^N$-trimerbody (10 ng) was added to all tubes, the tubes were briefly mixed and incubated at 25°C on a spiral mixer. After 6 h, the free labeled MFE23-scFv or $MFE23^N$-trimerbody in the supernatant was separated from cell-bound MFE23-scFv or $MFE23^N$-trimerbody by centrifugation followed by one wash with PBS. The cell pellets were finally counted for radioactivity using an automatic gamma counter (2470 Wizard, PerkinElmer). The reciprocal of the proportion of counts bound was plotted vs. the reciprocal of the cell dilution. Linear regression was performed using Graphpad Prism (version 7.03) and the immunoreactive fraction was obtained from the inverse of the intercept at the y-axis.

ELISA

The ability of unlabeled or ^{124}I-labelled MFE23-scFv and $MFE23^N$-trimerbody to bind CEA was analyzed by ELISA as previously described, with minor modifications.[23] In brief, Maxisorp (NUNC Brand Products, Roskilde, Denmark) plates were coated (0.3 µg/well) with human CEA (Sigma-Aldrich) and after washing and blocking with 200 µl 5% BSA in PBS, 100 µl with indicated amount of protein was added for 1 hour at room temperature. After three washes, 100 µl of anti-myc 9E10 mAb (1 µg/ml) were added for 1 hour at room temperature. After removal of detection antibody, 100 µl of horseradish peroxidase (HRP)-conjugated goat anti-mouse IgG (Fc specific; Sigma-Aldrich) were added for 1 hour at room temperature, after which the plate was washed and developed. Antigen titration was performed by triplicate with serial dilutions of both antibodies (concentration ranges 0.02-100 nM). Binding constants EC_{50} and Kd were

estimated from fitting curves to data using nonlinear regression according to the Graphpad Curve Fitting Guide (Graphpad Prism, version 6.01).

Animal studies: General aspects

Healthy female mice weighting 22±2 g (Balbc/Rj, 9 weeks, Janvier, Saint Berthevin, France) were used for *ex vivo* studies. Immunocompromised female mice weighting 28±2 g (NMRI-Foxn1^{nu}/Foxn1^{nu}, 9 weeks, Janvier) were used for tumor growing and *in vivo* PET studies. The animals were maintained and handled in accordance with the Guidelines for Accommodation and Care of Animals and internal guidelines. All experimental procedures were approved by the Ethical Committee of CIC biomaGUNE and the local authorities (Diputación Foral de Guipúzcoa).

Animal Tumor Model

For subcutaneous injection, both HT-1080 and MKN45 cells were harvested with trypsin/EDTA and resuspended in PBS supplemented with 10% basement membrane extract (Matrigel, Beckton Dickson, Franklin Lakes, NJ, USA). For tumor initiation, 2x10^6 HT-1080 or MKN45 cells were injected subcutaneously into one of the flanks of Foxn1^{nu}/Foxn1^{nu} nude mice (n=10 per cell line). During the procedure, mice were anesthetized with isofluorane. Tumor sizes were measured by using calipers on a weekly basis. From these measurements, tumor volume was estimated by V= L*W^2*0.5, where L is the tumor length and W is the tumor width. Six animals per cell line with similar tumor volume (370±77 mm^3 for HT-1080; 411±54 mm^3 for MKN45) were selected to be included in *in vivo* positron emission tomography studies.

Ex vivo biodistribution in mice

Animals (*n=4* per compound and time point) were anesthetized with isofluorane and a saline solution of ^{131}I-labeled MFE23-scFv or MFE23^N-trimerbody (average, 0.4 ± 0.1 MBq, 100 µl)

was injected through one of the lateral tail veins. At pre-determined time points (t=5 and 30 min, and 2, 6, 12, 18, 24 and 48 hours for the trimerbody; t= 5, 15 and 30 min, and 1, 2, 4, 8 and 18 hours for the scFv), animals were sacrificed by perfusion using saline solution, organs were quickly removed, rinsed with purified water and the amount of radioactivity was measured in an automatic gamma counter (2470 Wizard, PerkinElmer). The results were finally expressed as percentage of injected dose per gram of tissue (%ID/g). Urine and blood samples were also obtained just before perfusion. Part of the blood was processed to separate the plasma, which was used to perform the pharmacokinetic study. A fraction of the plasma and urine samples at t=12 hours were submitted to SDS-PAGE and TLC analysis, respectively, to identify the labeled species present.

Pharmacokinetic analysis

The plasma concentration of radioactivity versus time was analyzed by a compartmental method using non-linear regression.[24] Two kinetic models were compared.[25] First, the one-compartment model with bolus input and first-order elimination rate described by equation 1:

$$C(t) = \frac{D}{V} \cdot e^{-K_{el} * t} \quad \text{(eq. 1)}$$

Where D is the dose administered by intravenous injection; K_{el} is the elimination constant; and V is the distribution volume of distribution in the compartment. Apparent terminal half-life $(t_{1/2})$ is calculated as Ln2/K_{el} and the plasma clearance (Cl) for each compound is estimated as the ratio dose/AUC (area under the plasma concentration-time curve).

The second model was a two-compartment model with bolus input and first-order elimination rate, and is described by equation 2:

$$C(t) = A \cdot e^{-\alpha \cdot t} + B \cdot e^{-\beta \cdot t} \qquad \text{(eq.2)}$$

Where D is the dose administered; α and β are constants that depend solely on K_{12}, K_{21} (transfer constants between compartments 1 and 2) and K_{10} (elimination constant). V_c is the volume of distribution in the central compartment and V_{ss} is the total volume of distribution in steady-state. Apparent terminal half-life $(t_{1/2})$ is calculated as Ln2/β and the plasma clearance (Cl) for each compound is estimated as the ratio dose/AUC. Blood clearance (Cl_{blood}) was estimated from plasma clearance (Cl_{plasma}) using the following relation: $Cl_{blood} = Cl_{plasma}/BP$, where *BP* is the blood-to-plasma ratio. The initial estimates of the pharmacokinetic parameters were computed using the curve stripping technique by the add-in program PKSolver. The pharmacokinetic parameters were V_c and K_{el} in the case of one-compartment model and *A, B,* α and β for the two-compartment model. From these parameters, AUC ($D/V \cdot K_{el}$ and $A/\alpha + B/\beta$ for one- and two-compartmental model, respectively), Cl (D/AUC), V_{ss}, C_{max} (D/V and $A + B$ for one- and two-compartmental model, respectively), and apparent terminal half-life were determined. Appropriate weighting schemes (relative or Poisson) were applied according to the Graphpad Curve Fitting Guide. The Akaike information criterion (AIC) was used to identify the "best" model.[26]

PET scan procedures in mice

PET experiments ($n=3$ per tumor type and compound) were performed using an eXploreVista-CT small animal PET-CT system (GE Healthcare). Anesthesia was induced with 3-5% isoflurane and maintained by 1.5-2% of isoflurane in 100% O_2. To perform the studies, ^{124}I-labeled MFE23-scFv or MFE23^{N}-trimerbody (2.4 ± 0.3 MBq, 150 µL) was injected *via* one of the lateral tail veins concomitantly with the start of the first whole body PET acquisition (energy window: 400-700 KeV; duration of the scan = 40 min). Imaging sessions were repeated at t=2.5, 5, 11, 21 and 48 hours for the MFE23^{N}-trimerbody; t= 2.5, 5, 11, and 20 hours for the MFE-scFv (duration

= 30 min per acquisition). After each PET acquisition, a CT scan (X-Ray energy: 40 kV, intensity: 140 μA) was performed for a later attenuation correction in the image reconstruction. Random and scatter corrections were also applied to the reconstructed image (2DOSEM iterative algorithm, 4 iterations). PET-CT images of the same animal were co-registered and analyzed using PMOD image processing tool. Volumes of interest (VOIs) were placed on tumors, major organs and muscle (the latter to determine tumor-to-muscle ratios), and time–activity curves (decay corrected) were obtained. For the determination of the tumor-to-blood ratios, a region of interest was drawn in the left ventricle to estimate the concentration of radioactivity in blood.

Statistical analysis

Statistical analyses were performed using two-tailed Student *t*-test. P values <0.05 were considered significant.

RESULTS

Production of CEA-targeted MFE23-scFv and MFE23^{N}-trimerbody.

The MFE23-scFv (30.4 kDa calculated from its amino acid sequence, 28.2 kDa without the signal sequence) is a monovalent antibody fragment formed by fusing the V_H and V_L chains by a Gly-Ser linker (Fig 1a). The MFE23^{N}-trimerbody is a trivalent homotrimer [$(scFv\text{-}TIE)_3$, 110 kDa][27] with each monomer consisting of the MFE23-scFv linked to the human collagen XVIII derived TIE domain (39.3 kDa calculated from its amino acid sequence, 36.8 kDa without the signal sequence) (Fig. 1b). The MFE23^{N}-trimerbody exists as a stable trimer due to the noncovalent association between the TIE domains.[28] Following production and purification of the MFE23-scFv and MFE23^{N}-trimerbody, the proteins were analyzed to confirm their purity and functionality prior to conjugation. The MFE23-scFv and the MFE23^{N}-trimerbody were >

95% pure and migrated as monomers of ≈30 kDa and ≈40 kDa, respectively, under reducing SDS–PAGE conditions (Fig. S2A).

The functionality of purified antibodies was demonstrated by ELISA against plastic immobilized human CEA. MFE23-scFv and MFE23^{N}-trimerbody bind CEA in a concentration-dependent manner, with EC_{50} values of ≈3.06 nM and ≈0.98 nM, respectively (Fig. S2B). The difference in EC_{50} values are expected due to the avidity effect. Both MFE23-scFv (Kd≈2.06 nM)[29] and MFE23^{N}-trimerbody (Kd≈0.93 nM) have high affinity for CEA (Fig. S2B). The ability of both antibodies to detect the CEA as a cell surface protein was studied by flow cytometry (Fig. S2C).

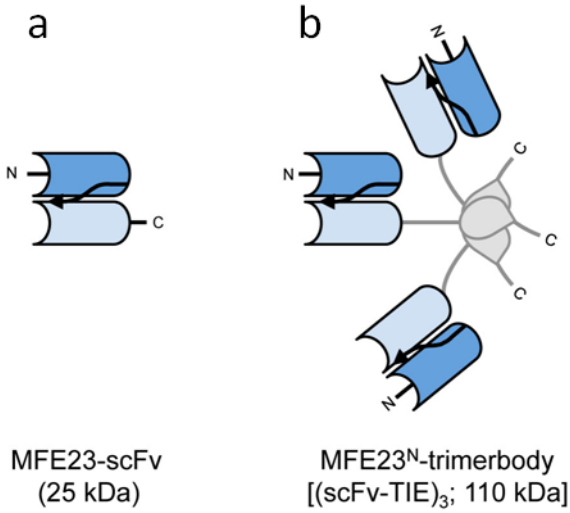

Figure 1. Schematic diagrams showing arrangement of V_H (dark blue) and V_L (light blue) domains in monomeric anti-CEA MFE23-scFv (a), and arrangement of V_H, V_L and collagen XVIII-derived trimerization domains (TIE, grey) in trimeric anti-CEA MFE23^{N}-trimerbody (b).

Radiolabeling of MFE23-scFv and MFE23^{N}-trimerbody.

Both the MFE23-scFv and the MFE23^{N}-trimerbody could be labeled with ^{131}I and ^{124}I. Overall decay-corrected radiochemical yields after purification were 47±8% for ^{131}I and 18±1% for ^{124}I

for the MFE23-scFv, and 41±12% for ^{131}I and 27±2% for ^{124}I for the MFE23^{N}-trimerbody. Radiochemical purities were above 95% in all cases at injection time (see Fig. S3 for an example of labeled MFE23^{N}-trimerbody before and after purification, and SDS-PAGE electrophoresis of the MFE23-scFv and the MFE23^{N}-trimerbody after purification). Specific activities of the labeled compounds were 3.3±0.5, 6.6±0.3, 2.9±0.8 and 9.9±0.7 MBq/μg for [^{131}I]MFE23-scFv, [^{124}I]MFE23-scFv, [^{131}I]MFE23^{N}-trimerbody and [^{124}I]MFE23^{N}-trimerbody, respectively. The labeled species showed good stability, with more than 95% of the radioactivity attached to the MFE23-scFv or MFE23^{N}-trimerbody after 24 hours of incubation both in physiologic saline solution and in mouse plasma at 37°C. Functional analysis showed that ^{124}I-labeled antibodies bound specifically to plastic immobilized human CEA, as determined by ELISA. The dose-dependent binding curves of [^{124}I]MFE23-scFv (EC_{50}≈2.87 nM) and [^{124}I]MFE23^{N}-trimerbody (EC_{50}≈0.99 nM) were comparable to unlabeled original antibodies (EC_{50}≈1.5 and ≈1.16 nM, respectively) (Fig. S4A). The Kd values of [^{124}I]MFE23-scFv (Kd≈2.23 nM) and [^{124}I]MFE23^{N}-trimerbody (Kd≈0.76 nM) were nearly identical in the binding to CEA to unlabeled antibodies (Kd≈1.7 nM and ≈1.10 nM respectively), indicating that there were no differences between affinities of non-radiolabeled or radiolabeled antibody fragments. In addition, the migration pattern of ^{124}I-labeled antibodies was consistent with the molecular weight of unlabeled proteins MFE23-scFv or MFE23^{N}-trimerbody (28 and 37 kDa, respectively) as estimated by visual inspection of reducing SDS-PAGE (Fig. S4B). The determination of the immunoreactive fraction showed values of 86 and 92% for [^{124}I]MFE23-scFv and [^{124}I]MFE23^{N}-trimerbody, confirming that they are still capable to bind to the target after radiolabeling.

Ex vivo biodistribution experiments

Accumulation of radioactivity in the different organs after intravenous administration showed similar trends for both protein scaffolds (Fig. 2 and Table S1). At short times (t=5 min) maximum accumulation of radioactivity was found in the kidneys (32.1±6.1 and 48.1±4.1 %ID/g for the MFE23^{N}-trimerbody and the MFE23-scFv, respectively) and in the liver (24.0±4.9 and 24.3±2.6%ID/g for the MFE23^{N}-trimerbody and the MFE23-scFv, respectively). The amount of radioactivity in both organs progressively decreased with time to reach values of 6.5±2.2 and 9.0±1.0 (kidneys) and 2.6±1.7 and 2.5±0.85 (liver) at t=12 hours for the MFE23^{N}-trimerbody and the MFE23-scFv, respectively. The high accumulation of radioactivity in the kidneys suggests elimination of the labeled species *via* urine, which was confirmed by the presence of radioactivity in this fluid at t>15 min. Indeed, accumulation of radioactivity in the urine increased over time and peaked at t=2 hours for both antibodies fragments to progressively decrease afterwards. TLC analysis of urine samples confirmed the presence of free iodide. Of note, plasma analyses performed at t=12 hours showed a migration pattern consistent with the molecular weight of unlabeled proteins, confirming that the presence of radioactivity in blood was due to the presence of the intact labeled protein scaffolds.

A significant accumulation of radioactivity was also observed in the spleen at short times after administration. In this organ, the concentration of radioactivity peaked at around 15-30 min after administration, with values of 24.3±1.6 and 16.7±2.5%ID/g (t=30 min) for the MFE23^{N}-trimerbody and the MFE23-scFv, respectively. This peak was followed by a rapid decrease. In parallel, progressive accumulation of radioactivity in the small intestine was observed for both antibodies. Altogether, these results suggest a combined elimination scheme with hepatobiliary excretion together with the above-mentioned urinary excretion.

A progressive accumulation of radioactivity in the thyroid gland was observed, peaking at t=480 min for MFE23-scFv and at t=720 for MFE23^{N}-trimerbody and suggesting a progressive de-iodination of the protein scaffolds. The very high accumulation of radioactivity in the stomach, which peaked at t=120 min and t=360 min for MFE23-scFv and MFE23^{N}-trimerbody, respectively (accumulation values of 39.8±8.2 and 28.2±9.0% ID/g, respectively), was also expected for both protein scaffolds, as this is the natural site for iodine metabolism.[30]

Accumulation in other major organs was relatively small. Some accumulation was observed for both compounds in the lungs at short times after administration. Accumulation in the brain was negligible, with values below 0.3%ID/g, irrespective of the antibodies and time point. Although antibody fragments crossing the blood brain barrier cannot be discarded, these low values might be due to the contribution of a small amount of blood that remains in the blood vessels after reperfusion.

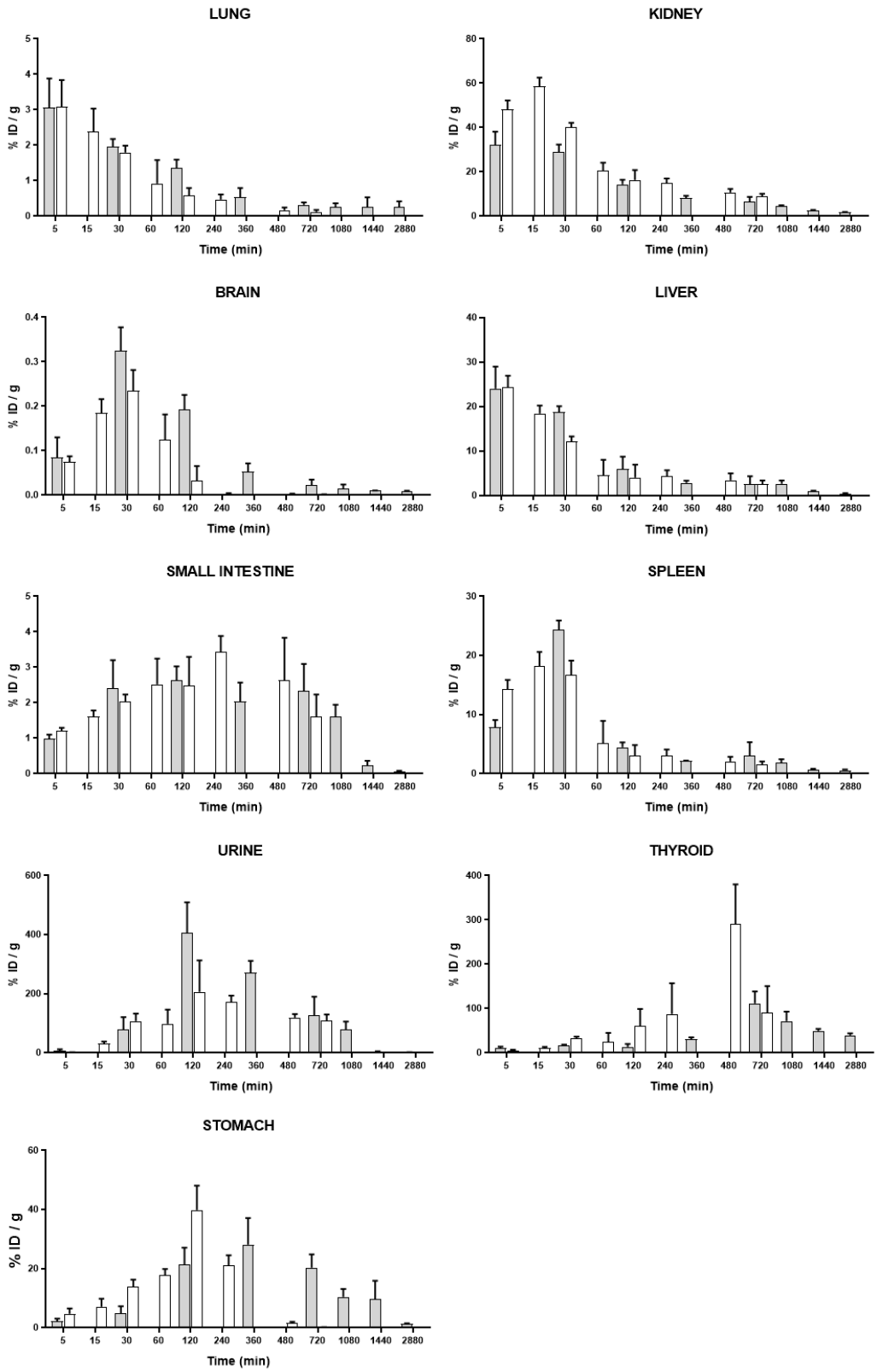
LUNG
KIDNEY
BRAIN
LIVER
SMALL INTESTINE
SPLEEN
URINE
THYROID
STOMACH
% ID / g
Time (min)
5 15 30 60 120 240 360 480 720 1080 1440 2880

Figure 2. Accumulation of ^{131}I-MFE23^{N}-trimerbody (grey bars) and ^{131}I-MFE23-scFv (white bars) in the different organs at different time points after intravenous administration, obtained by dissection and gamma counting. Results are expressed as percentage of injected dose per gram (mean ± standard deviation, n=4 per antibody and time point).

Pharmacokinetic study

The Akaike information criterion (AIC) values were 4.66 and -4.23 for one and two-compartment of ^{131}I-labeled MFE23^{N}-trimerbody, respectively, and 21.00 and -2.04 for one and two-compartment of ^{131}I-labeled MFE23-scFv. Thus, the disposition of both antibodies was better explained through a 2-compartment model (see Table 1).

Table 1. Main ^{131}I-labeled MFE23-scFv or MFE23^{N}-trimerbody pharmacokinetic parameters estimated using a 2-compartment model (equation: $C(t)=A\cdot e^{(-\alpha\cdot t)}+B\cdot e^{(-\beta\cdot t)}$).

Parameter	^{131}I-MFE23-scFv	^{131}I-MFE23^{N}-trimerbody
A (%ID/mL)	31.20	61.80
B (%ID/mL)	7.19	12.12
α (h^{-1})	3.93	2.22
β (h^{-1})	0.217	0.167
AUC (%ID.h/mL)	41.12	115.83
$t_{1/2}$ α (h)	0.18	0.32
$t_{1/2}$ β (h)	3.20	4.16
Cl (mL/h)	2.43	0.86
V_{ss} (mL)	9.18	3.72

After intravenous administration, both MFE23-scFv and MFE23^{N}-trimerbody pharmacokinetic profiles were biphasic with a rapid distribution phase ($t_{1/2}\alpha$=0.18 hours and 0.32 hours for MFE23-scFv and MFE23^{N}-trimerbody, respectively) and a slower elimination phase ($t_{1/2}\beta$= 3.20 hours and 4.16 hours for MFE23-scFv and MFE23N-trimerbody, respectively) (Fig. 3). The MFE23^{N}-trimerbody showed slower plasma clearance than the MFE-scFv (0.86 mL/hour versus 2.43 mL/hour). As the blood-to-plasma ratio was 0.66 and 0.65 for ^{131}I-labeled MFE23-scFv and MFE23^{N}-trimerbody, respectively, the blood clearance values were 3.93 and 1.44 L/day/Kg for ^{131}I-labeled MFE23-scFv and MFE23^{N}-trimerbody, respectively.

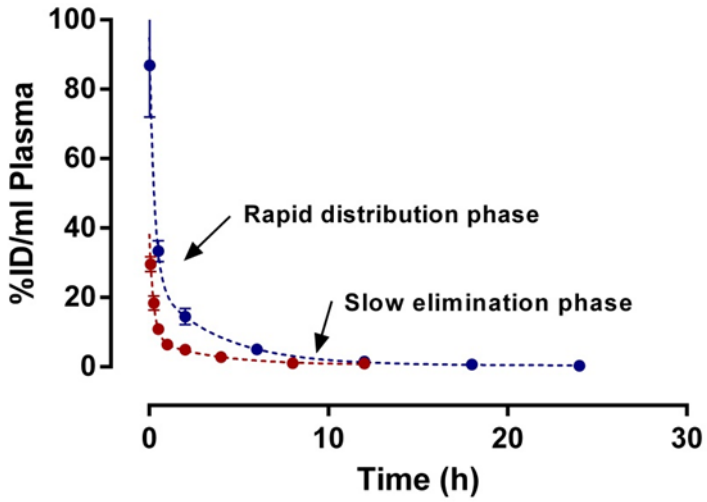

Figure 3. Pharmacokinetic profiles expressed as% ID.mL^{-1} in plasma vs. time of ^{131}I-MFE23-scFv (red) and ^{131}I-MFE23^{N}-trimerbody (blue).

In vivo PET studies

PET images obtained after intravenous administration of both protein scaffolds in CEA-negative and CEA-positive tumor models showed that accumulation of MFE23-scFv was lower than that of the MFE23^{N}-trimerbody for the same type of tumor (Fig. 4), irrespective of the time point (see Fig. 5 for representative images).

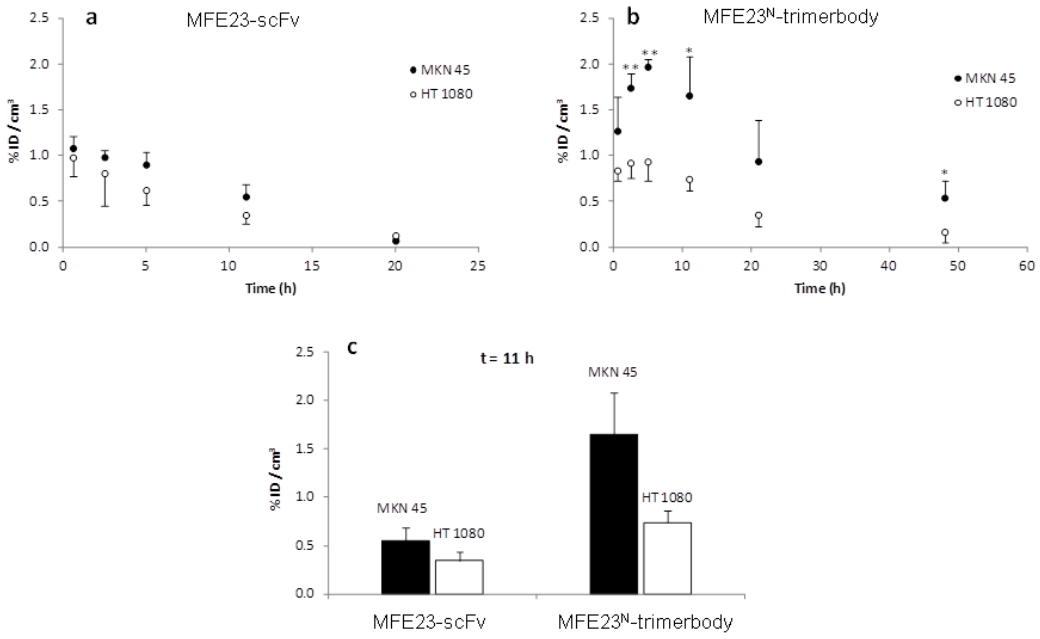

Figure 4. Accumulation of ^{124}I-MFE23-scFv (a) and ^{124}I-MFE23^{N}-trimerbody (b) in two different tumor types generated by subcutaneous injection of CEA-positive MKN45 (black dots) and CEA-negative HT1080 (white dots) cells, at different time points after administration; (c) Values at one selected time point (t=11 hours after administration), determined for the two protein scaffolds in the two different tumor types. Values are expressed as mean ± standard deviation, *n*=3 per compound, tumor type and time point; *p<0.05; **p<0.01.

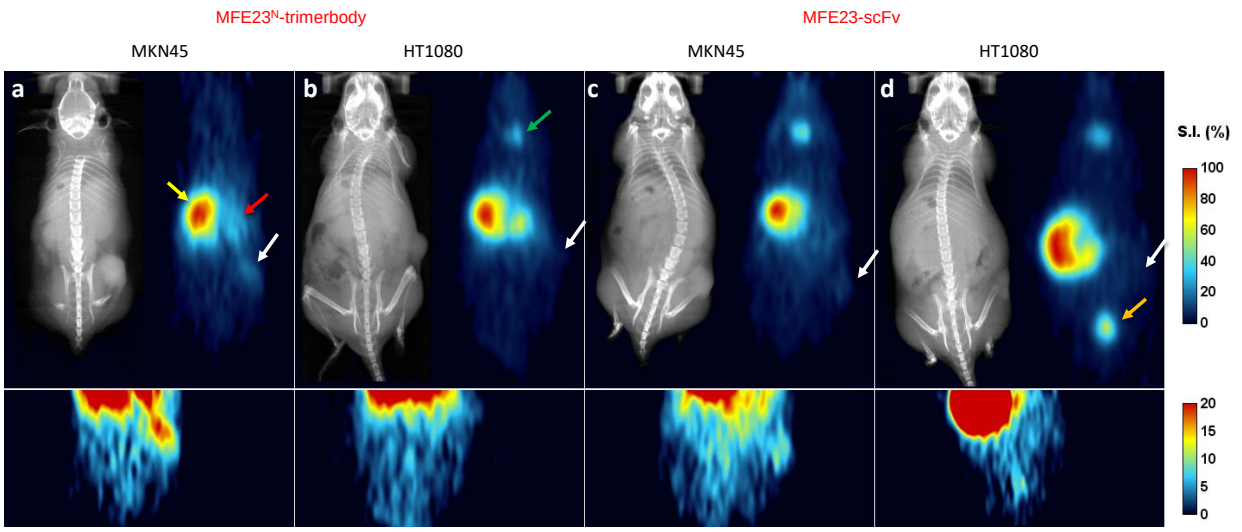

Figure 5. Top: Representative PET images (coronal slices) showing the distribution of the labeled species at t=11 hours after intravenous administration of ^{124}I-MFE23-scFv and ^{124}I-MFE23^{N}-trimerbody in mice bearing tumors: a) and b) MFE23^{N}-trimerbody in MKN45 and HT1080 tumor xenografts, respectively; c) and d) MFE23-scFv in MKN45 and HT1080 tumor xenografts, respectively. CT images are also shown for better localization of the organs (white arrow: tumor; yellow arrow: stomach; green arrow: thyroid gland; red arrow: liver; orange arrow: bladder). Bottom: Magnification of the regions in the white rectangle to better resolve the tumor uptake and improve contrast.

The accumulation of the MFE23-scFv in the tumor progressively decreased with time, to reach almost negligible values at t=20 hours. For the MFE23^{N}-trimerbody, a peak in the MKN45 tumor uptake was observed at t=5 hours. The concentration of radioactivity in the tumor progressively decreased afterwards. Specific tumor accumulation of the MFE23^{N}-trimerbody in CEA-positive tumors was significantly higher than that observed for the CEA-negative tumor at t=2.5, 5 and 11 hours (p values of 0.0115, 0.0035 and 0.0241, respectively).

Tumor-to-blood and tumor-to-muscle ratios also showed increased values for MFE23^{N}-trimerbody with respect to MFE23-scFv (Fig. 6), and higher values were obtained for MKN45-

derived tumors with respect to HT1080-derived tumors, irrespective of the protein scaffold and time point. Maximum tumor-to-muscle ratios in MKN45 xenografts were achieved at t=11h in both cases, with values close to 1 and 3 for MFE23-scFv and MFE23^{N}-trimerbody, respectively.

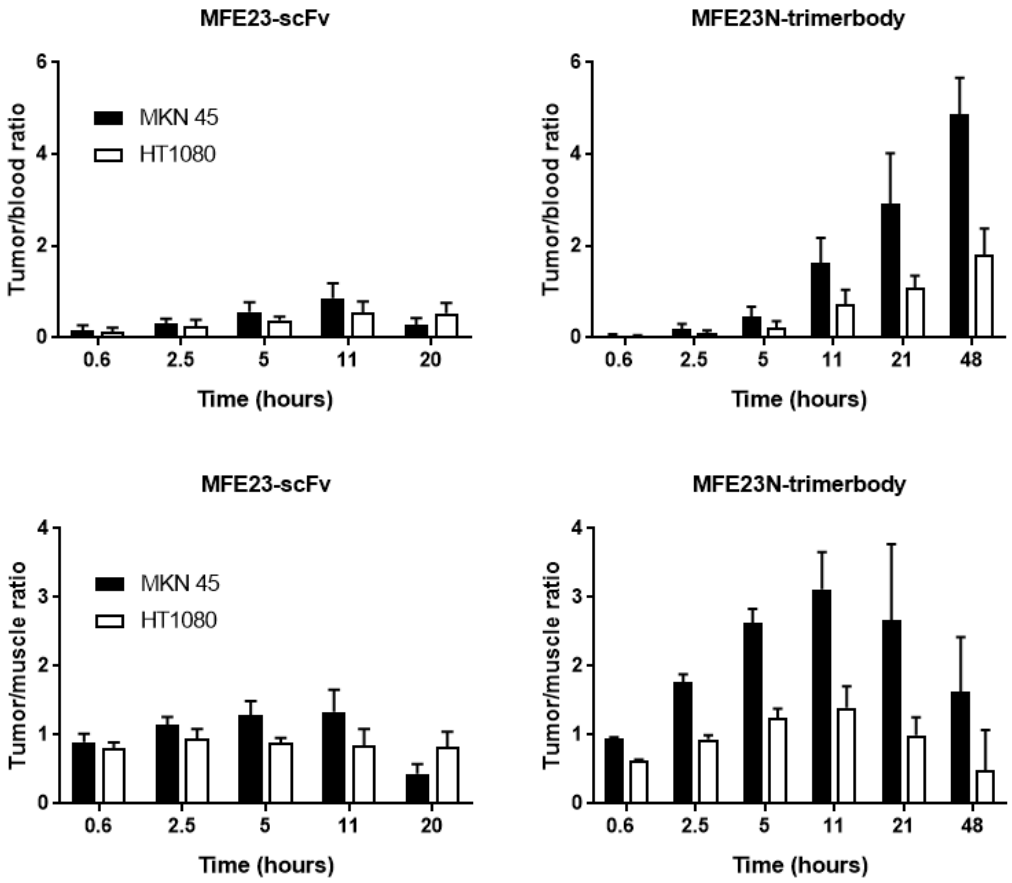

Figure 6. Tumor-to-blood (top) and tumor-to-muscle (bottom) ratios at different time points after intravenous administration of ^{124}I-MFE23-scFv and ^{124}I-MFE23^{N}-trimerbody in MKN45 and HT1080 tumor xenografts.

PET studies performed on tumor-bearing animals also provided the opportunity to assess the biodistribution of the labeled species *in vivo* and at the whole body level (Fig. S5). For both

molecules, similar biodistribution patterns to those observed *ex* vivo were obtained, with no apparent differences between the two protein scaffolds.

DISCUSSION

Monoclonal antibodies have long been considered attractive candidates for targeted therapy and diagnostics due to their highly specific targeting ability. A major disadvantage of using intact IgG antibodies as imaging probes is that they circulate in the blood for several days. The interaction of the Fc domain with the neonatal Fc receptor (FcRn) protects IgG from degradation and results in a long half-life of this class of antibodies in the blood.[31] Imaging studies carried out with Fab and $F(ab')_2$ fragments early evidenced that clearance and tumor penetration could be enhanced by using smaller antibody fragments.[32-33] Because of this, many engineered antibody fragments with different size and valence have been generated,[12, 34] being scFv one of the first options to be explored. Indeed, scFvs retain the specificity of the original antibody, but present a faster clearance,[5] with terminal half-lives in the range of a few hours and most of the activity cleared with the half-life of $T_{1/2}\alpha$.[35-36] The biodistribution pattern of scFvs in rodents is characterized by modest accumulation in the liver, low accumulation in brain and lungs and significant elimination via urine.[35, 37]

Here, we first investigated the biodistribution pattern of MFE23-scFv in wild type animals. With that aim, we decided to radiolabel the protein scaffold with ^{131}I and perform dissection and gamma counting experiments. For the radioiodination, different approaches both applied to intact IgG antibodies[38-39] and antibody fragments[40] have been reported, showing a method-dependent accumulation of radioiodinated antibody fragments in tumor xenografts. However, none of the labeling methods has shown clear advantages in terms of the subsequent evaluation *in vivo*[41] and direct radioiodination has shown preserved immunoreactivity in anti-CEA scFv-Fc variants.[42]

Hence, we selected this method for our studies. The conditions assayed in terms of incubation time and temperature resulted in moderate yields, but the amount of radioactivity obtained was sufficient to approach *ex vivo* and *in vivo* studies. Hence, no further optimization of the experimental conditions was carried out. ELISA experiments demonstrated that the labeling process did not have an impact on the biological function of the MFE23-scFv. The labeled species proved excellent stability both in physiologic saline solution and in mouse plasma over 24 hours, and also showed preserved immunoreactivity. These results are in good agreement with those obtained for other radioiodinated protein scaffolds previously reported in the literature and labeled using the same method,[43-44] and confirm the suitability of the labeled scFv to tackle *ex vivo* and *in vivo* experiments.

Our results showed a distribution pattern and blood pharmacokinetic parameters in good agreement with previous results,[35, 37] with elimination *via* urine and moderate accumulation in the liver, spleen and gastrointestinal tract (Fig. 2), suggesting a combined hepatobiliary/urinary excretion pattern, and fast blood clearance with $T_{1/2}\alpha$ and $T_{1/2}\beta$ values of 0.18 and 3.20 hours, respectively (Table 1).

PET images in tumor-bearing mice with the ^{124}I-labeled MFE23-scFv showed a high accumulation of radioactivity in the thyroid gland and also in the stomach (the latter also observed in *ex vivo* results), which are the natural sites of iodine metabolism.[30] It has been shown that using a different radiolabeling approach, i.e. by attachment of the Bolton-Hunter reagent on lysine residues of antibody fragments, attenuates the uptake of free, metabolized radioiodine in thyroid and stomach, although uptake in the tumors is not enhanced.[45] In our case, accumulation of MFE23-scFv in both CEA-positive and CEA-negative was low, irrespective of the time point. The maximum accumulation in the tumor is observed during the first scan (covering from 0-40

min after administration), and the concentration of radioactivity in the tumor progressively decreases afterwards (Fig. 4a).

The monovalency of scFvs and the fast clearance are significant limitations to tumor retention. Because of that, different approaches to genetically engineer monovalent scFv into longer circulating, multivalent fragments with greater avidity have been pursued. One alternative to prolong circulation time while keeping bivalency consists of creating a scFv-C_H3 covalent dimer (minibody), which results in increased molecular weight with respect to scFvs but also lacks interaction with FcRn, resulting in half-lives in the range 5-11 hours thus providing excellent tumor targeting capabilities.[33, 46] Alternatively, tumor avidity has also been improved by the constructions of diabodies, which consist of scFv dimers created by shortening the linker in scFv fragments in such a way that the domains cannot self-pair and are forced to cross associate. If the linker is further shortened, scFv association into trimers or tetramers can be forced.[47]

Here, we decided to investigate the pharmacokinetics and tumor targeting capacity of the recently reported CEA-specific MFE23 scFv-based N-terminal trimerbody. The radiolabeling was tackled following a parallel approach to that used for the scFv, again resulting in moderate labeling yields and excellent *in* vitro stability of the radiolabel. The distribution pattern in wild type animals followed a similar trend to that observed for the MFE23-scFv, with elimination mainly *via* urine and accumulation in liver, spleen and to a lesser extent in lungs. Contrary to the scFv, the MW of the $MFE23^N$-trimerbody is above the kidney filtration threshold, avoiding a potential problem of high kidney retention due to the reabsorption process in the kidney glomeruli. However, no significant differences between the two protein scaffolds are observed probably due to metabolism of the radiolabel within the glomeruli.[48] The pharmacokinetic study showed values of $T_{1/2}\alpha$ and $T_{1/2}\beta$ of 0.32 and 4.16 hours, respectively, resulting in a clearance

value of 0.86 ml/hour, which is significantly lower than the value obtained for the MFE23-scFv (2.43 ml/h), confirming that the scFv is cleared rapidly when compared to the scFv-based N-terminal trimerbody. Values obtained for the trimerbody are quite similar to those previously reported in the literature for $F(ab')_2$ fragments, which have similar molecular weight (100 kDa). For example, $T_{1/2\beta}$ and clearance values of 2.25 ± 0.02 h and 0.300 ± 0.007 mL/h were found in mice for a $F(ab')_2$ fragment of 7A7 mAb after intravenous administration in wild type mice.[49] Similar blood clearance properties were also reported for the $F(ab')_2$ fragments of IgG1.[50]

In vivo studies showed that the ^{124}I-labeled MFE23^{N}-trimerbody also accumulated in thyroid gland and in stomach, as expected, irrespective of the tumor model. Absolute quantification of the images for these organs has not been carried out, as the resulting values would be subjected to significant error due to partial volume effect (thyroid) and difficulties in delineation of the volume of interest on the CT images (thyroid and stomach). Interestingly, accumulation in the CEA-positive tumors was observed, with a maximum in tumor uptake at t=5 hours after administration. The value at the maximum, which was close to 2% ID/cm^3, was statistically higher than the accumulation of the labeled MFE23^{N}-trimerbody in the CEA-negative tumors (p value of 0.0035). This difference was also evident when the T/M ratios for both protein scaffolds and tumor models were analyzed. The T/M ratio for MFE23^{N}-trimerbody in the CEA-positive tumors peaked at t=11 hours (3.12±0.54), while the T/M ratio at the same time point in CEA-negative tumors was 1.39±0.31 (p value of 0.0087). At t=11 hours, the T/M ratio for the scFv is 1.33±0.32, significantly lower than the ratio obtained for the trimerbody (p value of 0.0078). These results confirm that the MFE23^{N}-trimerbody is selectively accumulated in CEA-positive tumors, and this uptake is higher than the one obtained for the corresponding scFv. The intermediate-sized and higher avidity of multivalent MFE23^{N}-trimerbody are important for

higher retention and slower tumor clearance. These results are also in good agreement with previous data obtained using optical imaging techniques.[14] Our previous studies show that, after intravenous injection of the Cy5-labeled trimerbody, maximum tumor uptake is achieved at 3 hours, whereas the signal intensity decreases by 24 hours and remains detectable for at least 48 hours.[14] Advantageously, the radiolabeling approach followed by *in vivo* PET imaging presented here can be translated into large animal species or even humans, facilitating thus the translation into the clinical setting.

In conclusion, we here demonstrate that the anti-CEA protein scaffolds MFE23-scFv and MFE23^{N}-trimerbody can be efficiently labeled with ^{124}I and ^{131}I without affecting the binding properties. Biodistribution studies demonstrate accumulation of the radioactivity in the liver, spleen, kidneys and urine, suggesting a combined hepatobiliary and urinary excretion. Pharmacokinetic investigation shows faster clearance of the MFE23-scFv. *In vivo* studies in tumor-bearing mice confirm that none of the antibodies selectively accumulates in CEA-negative tumors, while the MFE23^{N}-trimerbody selectively accumulates in the tumor when evaluated in a xenograft mouse model of CEA-positive gastric adenocarcinoma.

ASSOCIATED CONTENT

The following files are available free of charge.

Supplementary information containing Figures S1-S5 and Table S1 (PDF)

AUTHOR INFORMATION

Corresponding Author

*Paseo Miramón 182, 20014 San Sebastian, Guipuzcoa, Spain; e-mail: jllop@cicbiomagune.es; phone: +34943005333

Author Contributions

The manuscript was written through contributions of all authors. All authors have given approval to the final version of the manuscript. ‡These authors contributed equally.

Funding Sources

Spanish Ministry of Economy and Competitiveness (FATENANO, PCIN-2015-116)

Spanish Ministry of Economy and Competitiveness (CTQ2017-87637-R)

Danish Council for Independent Research, Medical Sciences (DFF-6110-00533)

ACKNOWLEDGMENT

Part of the work was funded by The Spanish Ministry of Economy and Competitiveness (FATENANO, PCIN-2015-116, and CTQ2017-87637-R) and performed under the Maria de Maeztu Units of Excellence Program from the Spanish State Research Agency – Grant No. MDM-2017-0720. LA-V was supported by the Danish Council for Independent Research, Medical Sciences (DFF -6110-00533).

REFERENCES

1. https://www.cancer.gov/about-cancer/understanding/statistics. (accessed December 06, 2017).
2. Nuñez-Prado, N.; Compte, M.; Harwood, S.; Álvarez-Méndez, A.; Lykkemark, S.; Sanz, L.; Álvarez-Vallina, L. The coming of age of engineered multivalent antibodies. *Drug Discov. Today* **2015,** *20* (5), 588-594.

3. Yazaki, P. J.; Wu, A. M. Construction and characterization of minibodies for imaging and therapy of colorectal carcinomas. *Methods in molecular biology (Clifton, N.J.)* **2003,** *207*, 351-364.
4. Beckman, R. A.; Weiner, L. M.; Davis, H. M. Antibody constructs in cancer therapy: Protein engineering strategies to improve exposure in solid tumors. *Cancer* **2007,** *109* (2), 170-179.
5. Knowles, S. M.; Wu, A. M. Advances in immuno-positron emission tomography: antibodies for molecular imaging in oncology. *J. Clin. Oncol.* **2012,** *30* (31), 3884-92.
6. Muyldermans, S., Nanobodies: Natural single-domain antibodies. In *Annu. Rev. Biochem.*, 2013; Vol. 82, pp 775-797.
7. Holliger, P.; Hudson, P. J. Engineered antibody fragments and the rise of single domains. *Nat. Biotechnol.* **2005,** *23* (9), 1126-1136.
8. Viola-Villegas, N. T.; Sevak, K. K.; Carlin, S. D.; Doran, M. G.; Evans, H. W.; Bartlett, D. W.; Wu, A. M.; Lewis, J. S. Noninvasive imaging of PSMA in prostate tumors with89Zr-Labeled huJ591 engineered antibody fragments: The faster alternatives. *Mol. Pharm.* **2014,** *11* (11), 3965-3973.
9. Adams, G. P.; Tai, M. S.; McCartney, J. E.; Marks, J. D.; Stafford Iii, W. F.; Houston, L. L.; Huston, J. S.; Weiner, L. M. Avidity-mediated enhancement of in vivo tumor targeting by single-chain Fv dimers. *Clin. Cancer. Res.* **2006,** *12* (5), 1599-1605.
10. Hu, S. Z.; Shively, L.; Raubitschek, A.; Sherman, M.; Williams, L. E.; Wong, J. Y. C.; Shively, J. E.; Wu, A. M. Minibody: A novel engineered anti-carcinoembryonic antigen antibody fragment (single-chain Fv-CH3) which exhibits rapid, high-level targeting of xenografts. *Cancer Res.* **1996,** *56* (13), 3055-3061.
11. Blanco-Toribio, A.; Sainz-Pastor, N.; Álvarez-Cienfuegos, A.; Merino, N.; Cuesta, A. M.; Sánchez-Martín, D.; Bonet, J.; Santos-Valle, P.; Sanz, L.; Oliva, B.; Blanco, F. J.; Álvarez-Vallina, L. Generation and characterization of monospecific and bispecific hexavalent trimerbodies. *mAbs* **2013,** *5* (1), 70-79.
12. Sánchez-Arévalo Lobo, V. J.; Cuesta, Á. M.; Sanz, L.; Compte, M.; García, P.; Prieto, J.; Blanco, F. J.; Álvarez-Vallina, L. Enhanced antiangiogenic therapy with antibody-collagen XVIII NC1 domain fusion proteins engineered to exploit matrix remodeling events. *Int. J. Cancer* **2006,** *119* (2), 455-462.
13. Cuesta, Á. M.; Sánchez-Martín, D.; Blanco-Toribio, A.; Villate, M.; Enciso-Álvarez, K.; Alvarez-Cienfuegos, A.; Sainz-Pastor, N.; Sanz, L.; Blanco, F. J.; Álvarez-Vallina, L. Improved stability of multivalent antibodies containing the human collagen XV trimerization domain. *mAbs* **2012,** *4* (2), 226-232.
14. Cuesta, Á. M.; Sánchez-Martín, D.; Sanz, L.; Bonet, J.; Compte, M.; Kremer, L.; Blanco, F. J.; Oliva, B.; Álvarez-Vallina, L. In vivo tumor targeting and imaging with engineered trivalent antibody fragments containing collagen-derived sequences. *PLoS ONE* **2009,** *4* (4).
15. Conaghan, P. J.; Ashraf, S. Q.; Tytherleigh, M. G.; Wilding, J. L.; Tchilian, E.; Bicknell, D.; Mortensen, N. J. M. C.; Bodmer, W. F. Targeted killing of colorectal cancer cell lines by a humanised IgG1 monoclonal antibody that binds to membrane-bound carcinoembryonic antigen. *Br. J. Cancer* **2008,** *98* (7), 1217-1225.
16. Kontermann, R. E.; Martineau, P.; Cummings, C. E.; Karpas, A.; Allen, D.; Derbyshire, E.; Winter, G. Enzyme immunoassays using bispecific diabodies. *Immunotechnology* **1997,** *3* (2), 137-144.

17. Sanz, L.; Kristensen, P.; Russell, S. J.; Ramirez García, J.; Álvarez-Vallina, L. Generation and characterization of recombinant human antibodies specific for native laminin epitopes: Potential application in cancer therapy. *Cancer Immunol., Immunother.* **2001,** *50* (10), 557-565.
18. Compte, M.; Blanco, B.; Serrano, F.; Cuesta, Á. M.; Sanz, L.; Bernad, A.; Holliger, P.; Álvarez-Vallina, L. Inhibition of tumor growth in vivo by in situ secretion of bispecific anti-CEA × anti-CD3 diabodies from lentivirally transduced human lymphocytes. *Cancer Gene Ther.* **2007,** *14* (4), 380-388.
19. Chen, J.; Wang, M.; Joyce, A.; Defranco, D.; Kavosi, M.; Xu, X.; O'Hara, D. M. Comparison of succinimidyl [^{125}I]iodobenzoate with iodogen iodination methods to study pharmacokinetics and ADME of biotherapeutics. *Pharm. Res.* **2014,** *31* (10), 2810-2821.
20. Bailey, G. S. Labeling of peptides and proteins by radioiodination. *Methods Mol. Biol.* **1994,** *32*, 441-8.
21. Lindmo, T.; Bunn, P. A., [65] Determination of the True Immunoreactive Fraction of Monoclonal Antibodies after Radiolabeling. In *Methods Enzymol.*, 1986; Vol. 121, pp 678-691.
22. Algaeer, S.; Mather, S. J.; Theobald, A. E. Validation of an analytical method for assay of immunoreactivity of99mTechnetium-radiolabelled monoclonal antibodies. *Pharm. Pharmacol. Commun.* **1998,** *4* (6), 279-282.
23. Alvarez-Cienfuegos, A.; Nuñez-Prado, N.; Compte, M.; Cuesta, A. M.; Blanco-Toribio, A.; Harwood, S. L.; Villate, M.; Merino, N.; Bonet, J.; Navarro, R.; Muñoz-Briones, C.; Sørensen, K. M. J.; Mølgaard, K.; Oliva, B.; Sanz, L.; Blanco, F. J.; Alvarez-Vallina, L. Intramolecular trimerization, a novel strategy for making multispecific antibodies with controlled orientation of the antigen binding domains. *Scientific Reports* **2016,** *6*.
24. Brown, A. M. A step-by-step guide to non-linear regression analysis of experimental data using a Microsoft Excel spreadsheet. *Comput. Methods Programs Biomed.* **2001,** *65* (3), 191-200.
25. DeVane, C. L. Pharmacokinetics (2nd edn, revised and expanded), M. Gibaldi and D. Perrier (Vol. 15 of Drugs and the pharmaceutical sciences), Marcel Dekker, New York, 1982. *Biopharm. Drug Disposition* **1983,** *4* (2), 201-201.
26. Zhang, Y.; Huo, M.; Zhou, J.; Xie, S. PKSolver: An add-in program for pharmacokinetic and pharmacodynamic data analysis in Microsoft Excel. *Comput. Methods Programs Biomed.* **2010,** *99* (3), 306-314.
27. Blanco-Toribio, A.; Lacadena, J.; Nuñez-Prado, N.; Álvarez-Cienfuegos, A.; Villate, M.; Compte, M.; Sanz, L.; Blanco, F. J.; Álvarez-Vallina, L. Efficient production of single-chain fragment variable-based N-terminal trimerbodies in Pichia pastoris. *Microbial Cell Factories* **2014,** *13* (1).
28. Boudko, S. P.; Sasaki, T.; Engel, J.; Lerch, T. F.; Nix, J.; Chapman, M. S.; Bächinger, H. P. Crystal Structure of Human Collagen XVIII Trimerization Domain: A Novel Collagen Trimerization Fold. *J. Mol. Biol.* **2009,** *392* (3), 787-802.
29. Lee, Y. C.; Boehm, M. K.; Chester, K. A.; Begent, R. H. J.; Perkins, S. J. Reversible dimer formation and stability of the anti-tumour single-chain Fv antibody MFE-23 by neutron scattering, analytical ultracentrifugation, and NMR and FT-IR spectroscopy. *J. Mol. Biol.* **2002,** *320* (1), 107-127.
30. Olafsen, T.; Wu, A. M. Antibody Vectors for Imaging. *Semin. Nucl. Med.* **2010,** *40* (3), 167-181.

31. Roopenian, D. C.; Akilesh, S. FcRn: The neonatal Fc receptor comes of age. *Nature Reviews Immunology* **2007,** *7* (9), 715-725.
32. Stillebroer, A. B.; Franssen, G. M.; Mulders, P. F. A.; Oyen, W. J. G.; Van Dongen, G. A. M. S.; Laverman, P.; Oosterwijk, E.; Boerman, O. C. ImmunoPET imaging of renal cell carcinoma with 124I- and 89Zr-Labeled Anti-CAIX monoclonal antibody cG250 in mice. *Cancer Biother. Radiopharm.* **2013,** *28* (7), 510-515.
33. Vogel, C. A.; Bischof-Delaloye, A.; Mach, J. P.; Pèlegrin, A.; Hardman, N.; Delaloye, B.; Buchegger, F. Direct comparison of a radioiodinated intact chimeric anti-CEA MAb with its $F(ab')_2$ fragment in nude mice bearing different human colon cancer xenografts. *Br. J. Cancer* **1993,** *68* (4), 684-690.
34. Wu, A. M.; Senter, P. D. Arming antibodies: Prospects and challenges for immunoconjugates. *Nat. Biotechnol.* **2005,** *23* (9), 1137-1146.
35. Wu, A. M.; Chen, W.; Raubitschek, A.; Williams, L. E.; Neumaier, M.; Fischer, R.; Hu, S. Z.; Odom-Maryon, T.; Wong, J. Y. C.; Shively, J. E. Tumor localization of anti-CEA single-chain Fvs: Improved targeting by non-covalent dimers. *Immunotechnology* **1996,** *2* (1), 21-36.
36. Evans, L.; Hughes, M.; Waters, J.; Cameron, J.; Dodsworth, N.; Tooth, D.; Greenfield, A.; Sleep, D. The production, characterisation and enhanced pharmacokinetics of scFv-albumin fusions expressed in Saccharomyces cerevisiae. *Protein Expression Purif.* **2010,** *73* (2), 113-124.
37. Kubaštová, H.; Kleinová, V.; Seifert, D.; Fišer, M.; Kranda, K. Radioiodination and biodistribution of the monoclonalantibody TU-20 and its SCFV fragment. *Czechoslovak Journal of Physics* **2006,** *56* (SUPPL. 4), D683-D688.
38. Reist, C. J.; Archer, G. E.; Wikstrand, C. J.; Bigner, D. D.; Zalutsky, M. R. Improved targeting of an anti-epidermal growth factor receptor variant III monoclonal antibody in tumor xenografts after labeling using N- succinimidyl 5-iodo-3-pyridinecarboxylate. *Cancer Res.* **1997,** *57* (8), 1510-1515.
39. Shankar, S.; Vaidyanathan, G.; Affleck, D. J.; Peixoto, K.; Bigner, D. D.; Zalutsky, M. R. Evaluation of an internalizing monoclonal antibody labeled using N-succinimidyl 3-[^{131}I]iodo-4-phosphonomethylbenzoate ([^{131}I]SIPMB), a negatively charged substituent bearing acylation agent. *Nucl. Med. Biol.* **2004,** *31* (7), 909-919.
40. Pruszynski, M.; Kang, C. M.; Koumarianou, E.; Vaidyanathan, G.; Zalutsky, M. R. D-amino acid peptide residualizing agents for protein radioiodination: Effect of aspartate for glutamate substitution. *Molecules* **2018,** *23* (5).
41. Shankar, S.; Vaidyanathan, G.; Kuan, C. T.; Bigner, D. D.; Zalutsky, M. R. Antiepidermal growth factor variant III scFv fragment: Effect of radioiodination method on tumor targeting and normal tissue clearance. *Nucl. Med. Biol.* **2006,** *33* (1), 101-110.
42. Kenanova, V.; Olafsen, T.; Williams, L. E.; Ruel, N. H.; Longmate, J.; Yazaki, P. J.; Shively, J. E.; Colcher, D.; Raubitschek, A. A.; Wu, A. M. Radioiodinated versus radiometal-labeled anti-carcinoembryonic antigen single-chain Fv-Fc antibody fragments: Optimal pharmacokinetics for therapy. *Cancer Res.* **2007,** *67* (2), 718-726.
43. Kameswaran, M.; Samuel, G.; Dev Sarma, H.; Shinde, S. N.; Dash, A.; Venkatesh, M. ^{131}I-Nimotuzumab - A potential radioimmunotherapeutic agent in treatment of tumors expressing EGFR. *Appl. Radiat. Isot.* **2015,** *102*, 98-102.
44. Yang, C.; Yun, Q.; Sun, H.; Yang, G.; Liang, T.; Zhang, C.; Song, J.; Han, J.; Hou, G. Non-invasive imaging of toll-like receptor 5 expression using ^{131}I-labeled mAb in the mice bearing H22 tumors. *Oncology Letters* **2014,** *7* (6), 1919-1924.

45. Robinson, M. K.; Doss, M.; Shaller, C.; Narayanan, D.; Marks, J. D.; Adler, L. P.; Gonzalez Trotter, D. E.; Adams, G. P. Quantitative immuno-positron emission tomography imaging of HER2-positive tumor xenografts with an iodine-124 labeled anti-HER2 diabody. *Cancer Res.* **2005,** *65* (4), 1471-8.
46. Milenic, D. E.; Yokota, T.; Filpula, D. R.; Finkelman, M. A. J.; Dodd, S. W.; Wood, J. F.; Whitlow, M.; Snoy, P.; Schlom, J. Construction, Binding Properties, Metabolism, and Tumor Targeting of a Single- Chain Fv Derived from the Pancarcinoma Monoclonal Antibody CC49. *Cancer Res.* **1991,** *51*, 6363-6371.
47. Dolezal, O.; Pearce, L. A.; Lawrence, L. J.; McCoy, A. J.; Hudson, P. J.; Kortt, A. A. ScFv multimers of the anti-neuraminidase antibody NC10: Shortening of the linker in single-chain Fv fragment assembled in V(L) to V(H) orientation drives the formation of dimers, trimers, tetramers and higher molecular mass multimers. *Protein Eng.* **2000,** *13* (8), 565-574.
48. Li, L.; Bading, J.; Yazaki, P. J.; Ahuja, A. H.; Crow, D.; Colcher, D.; Williams, L. E.; Wong, J. Y.; Raubitschek, A.; Shively, J. E. A versatile bifunctional chelate for radiolabeling humanized anti-CEA antibody with In-111 and Cu-64 at either thiol or amino groups: PET imaging of CEA-positive tumors with whole antibodies. *Bioconjug. Chem.* **2008,** *19* (1), 89-96.
49. Rabasa Capote, A.; Gonzalez, J. E.; Rodriguez-Vera, L.; Lopez, A.; Sanchez Ramirez, B.; Garrido Hidalgo, G. Pharmacokinetics and Biodistribution Study of 7A7 Anti-Mouse Epidermal Growth Factor Receptor Monoclonal Antibody and Its F(ab')(2) Fragment in an Immunocompetent Mouse Model. *ISRN Pharmacol* **2012,** *2012*, 417515.
50. Covell, D. G.; Barbet, J.; Holton, O. D.; Black, C. D.; Parker, R. J.; Weinstein, J. N. Pharmacokinetics of monoclonal immunoglobulin G1, F(ab')2, and Fab' in mice. *Cancer Res.* **1986,** *46* (8), 3969-78.